Short communication

Photocatalyst ZnO-doped Bi_2O_3 powder prepared by spray pyrolysis

Chin-Yi Chen [a,*], Jui-Chung Weng [a], Jing-Heng Chen [b], Shih-Hsin Ma [b], Kun-Huang Chen [c], Tzyy-Leng Horng [d], Chien-Yie Tsay [a], Chi-Jung Chang [e], Chung-Kwei Lin [f], Jerry J. Wu [g]

[a] Department of Materials Science and Engineering, Feng Chia University, Taichung 407, Taiwan
[b] Department of Photonics, Feng Chia University, Taichung 407, Taiwan
[c] Department of Electrical Engineering, Feng Chia University, Taichung 407, Taiwan
[d] Department of Applied Mathematics, Feng Chia University, Taichung 407, Taiwan
[e] Department of Chemical Engineering, Feng Chia University, Taichung 407, Taiwan
[f] School of Dental Technology, College of Oral Medicine, Taipei Medical University, Taipei 110, Taiwan
[g] Department of Environmental Engineering and Science, Feng Chia University, Taichung 407, Taiwan

ARTICLE INFO

ABSTRACT

In the present study, nanocrystalline photocatalyst Bi_2O_3 powders with various ZnO additions were synthesized by spray pyrolysis at 600 (SP600) and 700 °C (SP700). The Bi_2O_3 powder converted from a monoclinic α phase to a tetragonal β phase at pyrolysis temperatures ≥ 600 °C. The crystallinity of the SP powder increased with the increase in pyrolysis temperature. The morphology of the SP powders was observed to reveal a porous structure. The photocatalytic activity of the Bi_2O_3-based powder strongly depends on its specific surface area. Based on a constant specific surface area, 5 mol% ZnO addition can significantly increase the photocatalytic efficiency of SP700 Bi_2O_3 powder from 46% to 86% under visible irradiation for 6 h. Intrinsically, the photocatalytic performance of the SP powder is affected by the crystallite size. Furthermore, the photocatalytic activity of the resulting powders was compared with that of the P25 powder (a commercialized TiO_2 powder). The mechanisms for the formations of the porous powders are also delineated.

© 2014 Elsevier B.V. All rights reserved.

1. Introduction

Numerous studies have been focusing on the efficiency of energy utilization to meet increasing energy demands. A primary source of energy is the sun. The use of solar energy with high efficiency and low energy exhaust is crucially important. Many researchers have focused on developing materials that can combine or cooperate with nature. The semiconductor photocatalyst, being a material of green technology, has thus received extensive interest from R&D in this related field due to its high efficiency in decomposing pollutants, such as toxic chemical compounds and bacteria [1].

At the end of the 1960s, TiO_2 was known for its ability to photocatalytically split water into hydrogen and oxygen. Nanostructured TiO_2 thus became the most common photocatalytic material due to its high photocatalytic activity, non-toxicity, low cost, and excellent physiochemical stability [2,3]. However, a drawback of TiO_2 in the photocatalytic process is that it must be excited by a light wavelength of less than 388 nm. That is, TiO_2 absorbs only the UV light region, ~4%

intensity in solar irradiation, but not the visible light and infrared light regions [4].

Bismuth oxide (Bi_2O_3), a new semiconductor photocatalyst with a direct band gap of ~2.3–2.8 eV, can absorb the visible light region to exhibit photocatalytic behavior. However, Bi_2O_3 can be a photocatalyst when its specific surface area is high. A Bi_2O_3 powder with micro-size grains may lengthen the distance of light-generated charge carriers (electron-hole pairs) transferring to the reaction surface, lowering the energy conversion efficiency due to recombination [5,6]. Zinc oxide (ZnO), also a semiconductor (band gap: ~3.2 eV) possessing several excellent physical properties, has been applied in electronic and optoelectronic devices in several studies [7,8]. In the present study, Bi_2O_3 powders with various amounts of ZnO added were synthesized from bismuth nitrate and zinc nitrate by SP. The structural properties of the as-pyrolyzed powders were characterized as a function of ZnO addition at different pyrolysis temperatures. The photocatalytic activities of the pyrolyzed powders were evaluated by degrading methylene orange under a visible light radiation system.

2. Experimental

The Bi_2O_3 powders with various amounts of ZnO added were synthesized from bismuth nitrate and zinc nitrate by SP in this study. Bismuth nitrate pentahydrate (BiNH, 98.0%, Alfa Aesar) and zinc nitrate

* Corresponding author at: Department of Materials Science and Engineering, Feng Chia University, 100, Wenhwa Road, Seatwen, Taichung, Taiwan 40724, Taiwan. Tel.: +886 4 24517250×5313; fax: +886 4 24510014.
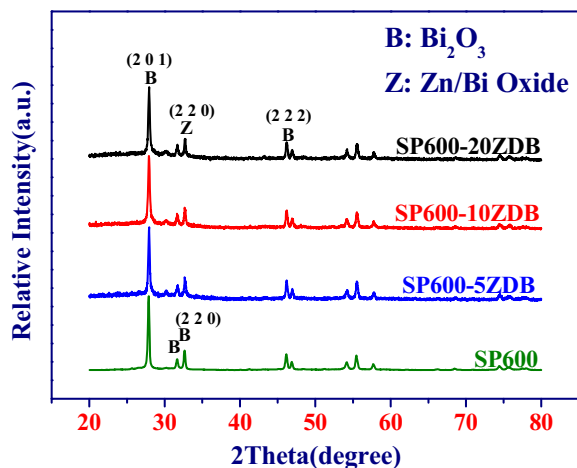E-mail address: chencyi@fcu.edu.tw (C.-Y. Chen).

Fig. 1. XRD patterns of SP600 Bi$_2$O$_3$ powders as a function of ZnO addition.

Table 1
Lattice constant, grain size and energy band gap of SP Bi$_2$O$_3$ powders as a function of ZnO addition. The powders spray pyrolyzed at 600 and 700 °C are denoted as SP600 and SP700, respectively.

		undoped	5ZDB	10ZDB	20ZDB
Lattice constant (nm)	SP600	0.7748	0.7736	0.7735	0.7733
	SP700	0.7747	0.7738	0.7735	0.7734
Crystallite Size (nm)	SP600	61.25 ± 7	61.51 ± 6	61.79 ± 7	63.44 ± 8
	SP700	64.19 ± 6	67.25 ± 6	71.64 ± 7	72.03 ± 4
Energy band gap (eV)	SP600	2.43	2.52	2.52	2.54
	SP700	2.38	2.51	2.51	2.53

in the range of 400–800 nm. The variation of the methylene orange concentration, determined by the transmittance of the solution at 454 nm, was evaluated by UV–vis spectrophotometry (U-2900, Hitachi, Japan). The band gap of the SP powders was calculated from UV–Vis diffuse reflectance spectroscopy (U-3900, Hitachi, Japan) using Tauc plots [9].

3. Results and discussion

Figs. 1 and 2 show the X-ray diffraction patterns of the SP600 and SP700 Bi$_2$O$_3$ powders as a function of ZnO addition, respectively. The powders pyrolyzed at temperatures ≥ 600 °C were identified as a tetragonal β-type Bi$_2$O$_3$ phase (JCPDS card no. 78-1793). No significant changes in Bi$_2$O$_3$ phase were found from the XRD patterns of the powders pyrolyzed at 600 and 700 °C. However, note that the diffraction peaks at plane (2 2 0) shifted slightly to higher angles as the ZnO was added. The diffraction patterns identified the SP ZnO-doped Bi$_2$O$_3$ powders as a Zn/Bi oxide phase (JCPDS card no. 43-0449). The changes in diffraction angle increased with increases in ZnO addition. This suggests that ZnO addition may lower the lattice constant of SP Bi$_2$O$_3$. It is likely that since the ionic radius of Zn^{2+} (0.74 Å, coordination number (CN) = 6) is smaller than that of Bi^{3+} (1.17 Å, CN = 6), Zn^{2+} ions can partially substitute for the sites of Bi^{3+} ions. As a result, a nonstoichiometric solid solution can be expected to form in the Bi–oxide matrix.

Table 1 shows the lattice constant of the Bi$_2$O$_3$ powders pyrolyzed at 600 and 700 °C as a function of ZnO content. In comparison with the theoretical values, no significant differences in the lattice parameters of the unadded powders were found after SP, implying that relatively pure phases of the Bi$_2$O$_3$ powders were obtained. The lattice constant of SP Bi$_2$O$_3$ powders decreased when the ZnO was added, implying that the ZnO dissolved into the lattice structure of the Bi$_2$O$_3$ matrix. Furthermore, the crystallite sizes of the Bi$_2$O$_3$ powders pyrolyzed at 600 and 700 °C as a function of ZnO addition are listed in Table 1. The crystallite size increased with the increase in pyrolysis temperature.

hexahydrate (ZNH, 99.0%, Showa) were first dissolved homogeneously in acetic acid (100%, Scharlau) at room temperature by stirring. The resulting solution was added into deionized water to obtain precursor solution for SP. The concentration of the precursor solution was prepared as 1 wt%. The chemical formulas of BiNH, ZNH and acetic acid are Bi(NO$_3$)$_3$· 5H$_2$O, Zn(NO$_3$)$_2$· 6H$_2$O and CH$_3$COOH, respectively. The chemicals were all reagent grade. The obtained precursor solution was atomized into small drops by an ultrasonic nebulizer with a resonant frequency of 1.65 MHz (King Ultrasonics Co., Ltd., Taipei, Taiwan). The atomized precursor drops were then transported into a tubular furnace by carrier air for SP at various pyrolysis temperatures. The pyrolysis temperatures were 600 and 700 °C; the resulting powders were thus denoted as SP600 and SP700, respectively.

The phase identification was performed by X-ray diffractometry (XRD, Rigaku D/MAX2500). The morphology of as-pyrolyzed powders was observed using field emission scanning electronic microscopy (FE-SEM, JSM-6700 F, JEOL). The surface area (BET) measurements were carried out using a HORIBA SA-9600 series Surface Area Analyzer, employing nitrogen gas adsorption. The photocatalytic activities of the pyrolyzed powders were evaluated by degrading methylene orange (C$_{14}$H$_{14}$N$_3$NaO$_3$S, 20 ppm, 160 ml) under a visible light radiation system (HMLS-Xenon 350 W, HMT Co., Taiwan). The as-pyrolyzed powder was dispersed into an aqueous solution containing methylene orange. The distance between the visible light source and aqueous solution was set to 15 cm. The wavelength of the visible light source, xenon arc lamps with optical filtration (FEL0400, THORLABS Inc., USA), was
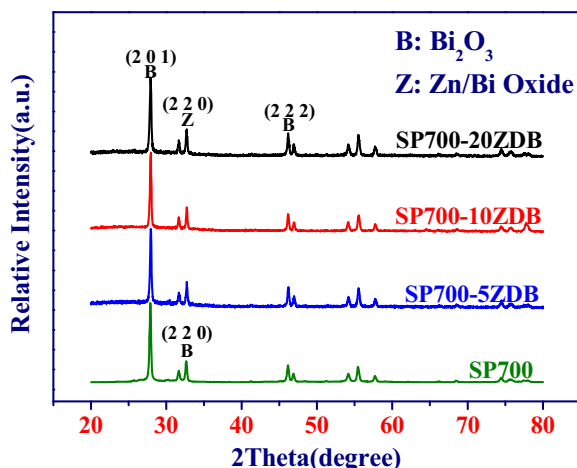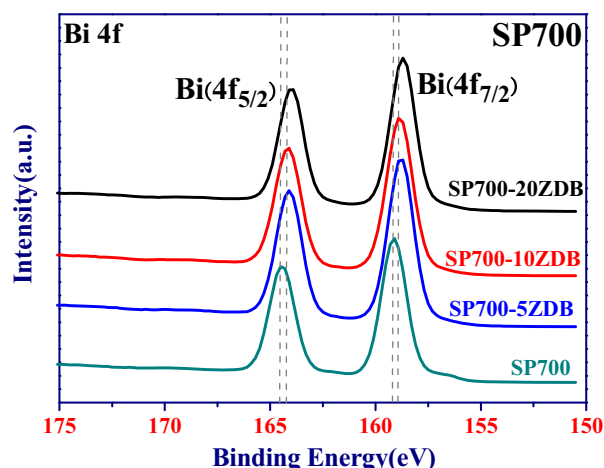

Fig. 2. XRD patterns of SP700 Bi$_2$O$_3$ powders as a function of ZnO addition.

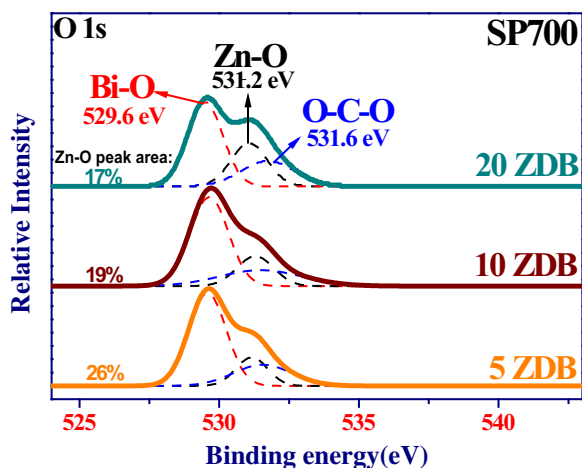**Fig. 3.** Bi 4f XPS spectra for SP700 Bi$_2$O$_3$ powders as a function of ZnO additions.

Fig. 4. O 1s XPS spectra and their Gaussian-resolved components for SP700 Bi_2O_3 powders with various ZnO additions (solid line: experimental data, dashed line: Gauss fitting).

The dissolution of ZnO in Bi_2O_3 matrix may cause the formation of oxygen vacancies that enhance the ionic transportation during pyrolysis. The increase in oxygen vacancies can be explained by the following reaction:

$$2ZnO \xrightarrow{Bi_2O_3} 2Zn'_{Bi} + V_O^{\bullet\bullet} + 2O_O^x$$

The formation of oxygen vacancies, regarded as point defects, facilitates the diffusion rate of ions during SP [10]. The higher the diffusion rate of ions, the greater the rate of grain growth of ceramics. The ZnO addition thus increased the crystallinity of the SP Bi_2O_3 powder. The band gaps of SP Bi_2O_3 powders as a function of ZnO addition are also listed in Table 1. Note that the band gaps of the SP Bi_2O_3 powders were increased by adding ZnO. However, no significant differences in the band gap can be found between the ZnO-added Bi_2O_3 powders.

This shows a trend similar to the lattice constant as a function of ZnO addition.

Fig. 3 shows the Bi 4f XPS spectra for SP700 Bi_2O_3 powders as a function of ZnO additions. Both the Bi 4f peaks of the SP Bi_2O_3 powder shifted slightly to lower binding energies when ZnO was added. The valance of bismuth ion decreased due to the addition of ZnO, suggesting the dissolution of ZnO in the Bi_2O_3 matrix. Furthermore, Fig. 4 shows the O 1s XPS spectra and their Gaussian-resolved components for SP700 Bi_2O_3 powders as a function of ZnO additions. The ZnO component can be noted in the O 1s spectra. The area under the ZnO curve increased with increases in ZnO addition. In contrast, the area under BiO component decreased when the ZnO addition was increased. This suggests the presence of ionic zinc in the Bi_2O_3 matrix. The analyses in Fig. 3 and 4 show good agreement with the results of the XRD data.

Figs. 5 and 6 show the FE-SEM micrographs of the Bi_2O_3 powders pyrolyzed at 600 and 700 °C, respectively, as a function of ZnO addition. Note that the pyrolyzed particles exhibited particulate morphology, being spherical in shape. Observed were three powder structures: solid, hollow, and irregular. The particles, which had an extremely small size of 50–200 nm, were identified as solid by TEM observation, as shown in the insets of the corresponding SEM micrographs. The extremely small drops tended to convert into solid particles due to the rapid, very small amounts of solvent evaporation. They were produced from the BiNH precursor via a one-particle-per-drop mechanism during SP [11], as shown in Fig. 7. The atomized BiNH precursor drops underwent solvent evaporation, solute precipitation, and subsequent solid oxide formation. This resulted in the formation of solid and hollow structures of the Bi_2O_3 powder. The particle sizes of the SP Zn/Bi oxide powders resulting from different formation mechanisms are listed in Tables 2 and 3. Larger drops formed into hollow structured particles with a size of 200–1000 nm due to the surface precipitation of the solute. Some fractured particles were also found in the SP powders, showing evidence of surface precipitation of the hollow particles. The particles exhibited a structure of nanoparticle clusters. That is, each porous irregular particle was composed of nanoparticles, which could have been precipitated in the precursor solution before atomization. As shown in Tables 2 and 3, the primary particle size of the SP Bi_2O_3 was significantly increased by the addition of ZnO. This may result
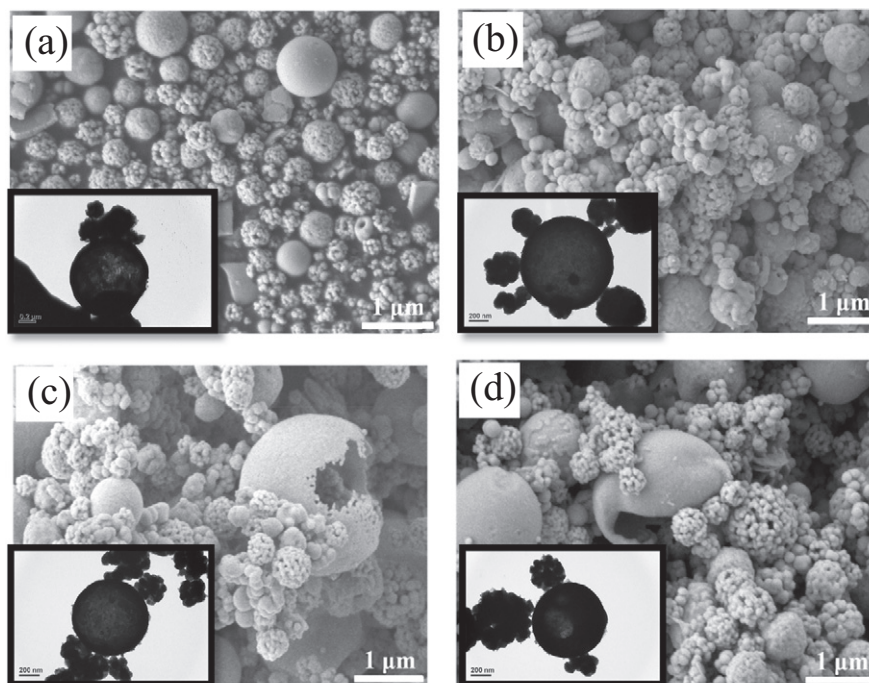

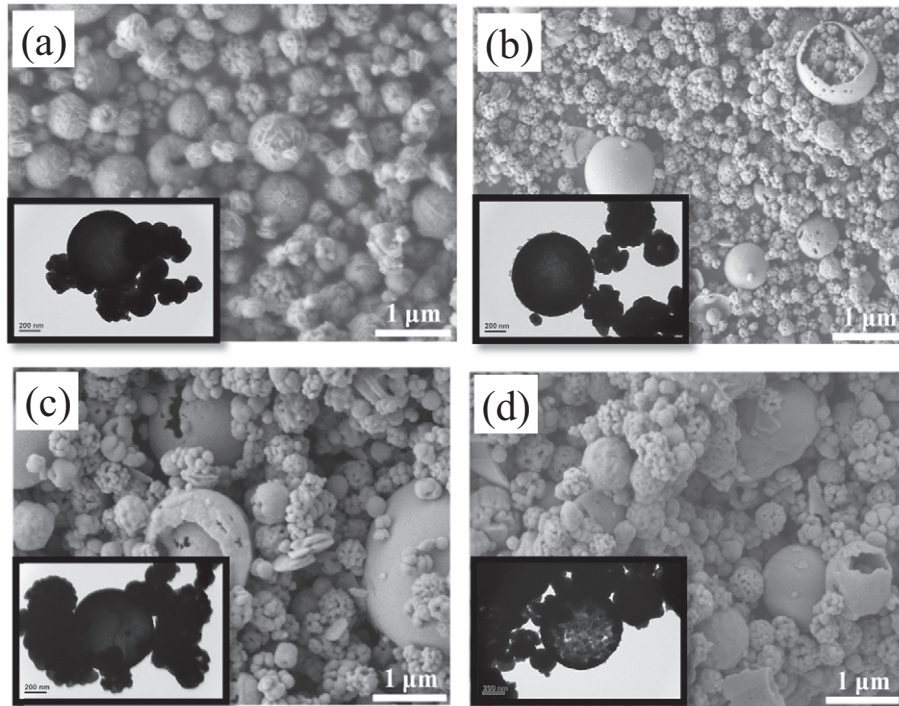**Fig. 5.** SEM micrographs of (a) undoped SP600 Bi_2O_3 powder, (b) 5 mol%, (c) 10 mol%, and (d) 20 mol% ZnO-doped SP600 Bi_2O_3 powders.

Fig. 6. SEM micrographs of (a) undoped SP700 Bi$_2$O$_3$ powder, (b) 5 mol%, (c) 10 mol%, and (d) 20 mol% ZnO-doped SP700 Bi$_2$O$_3$ powders.

from the rapid evaporation of precursors at higher temperature due to their very low melting points (~76 °C and < 110 °C for BiNH and ZNH, respectively), and deposition subsequently occurs on the surface of pre-cipitated particles during SP. In addition, coagulation of precursor drop-lets (or particles) could become more important when the particle is heated to above its melting temperature during the thermolysis and sintering stages of SP [12]. Note that in Fig. 7, the precipitated nanopar-ticles in the atomized drops were carried into the reaction furnace to undergo SP processes. The mechanism of nanoparticle agglomeration resulted in porous nanocrystalline particles during SP [13]. This nanoparticle-clustered structure revealed a high specific surface area

of the SP powders, which enhanced the photocatalytic activity of the Zn/Bi oxide powder.

The BET surface areas of the SP ZnO-doped Bi$_2$O$_3$ powders are listed in Table 4. Note that the specific surface areas of the powders pyrolyzed at 600 and 700 °C were decreased by adding small amounts of ZnO. The most likely reason is the formation of ionic defects arising from the ZnO addition, as shown in Table 1. Furthermore, a higher SP temperature may slightly lower the specific surface area of the SP powder due to the larger crystallite size, facilitated by ionic transportation during SP. This also shows good agreement with the results in Table 1. To eliminate the effect of surface area on the photocatalytic activity of the SP
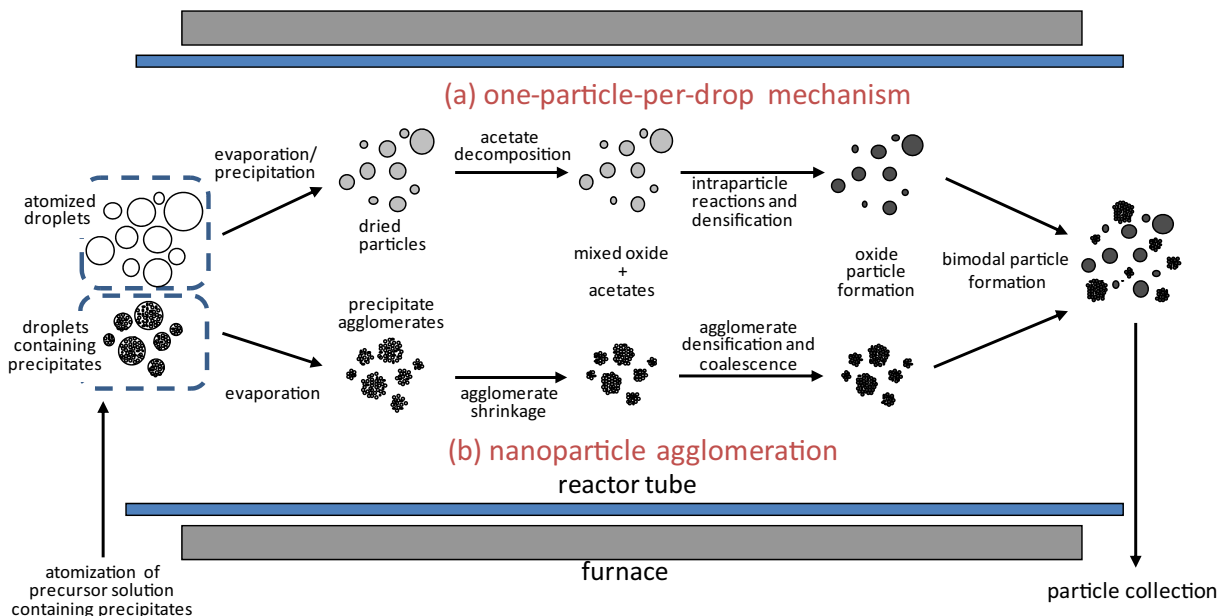

Fig. 7. Schematic diagram of mechanisms of Bi$_2$O$_3$ powder formation in spray pyrolysis.

Table 2
Particle sizes of SP600 Bi_2O_3 powders as a function of ZnO addition.

SP600	Mechanism of particle formation		
	One-particle-per-drop	Nanoparticle agglomeration	
	Mean particle size (nm)	Primary particle size (nm)	Secondary particle size (nm)
Undoped	938.2	74	601.5
5ZDC	991.2	131.7	536.3
10ZDC	977.5	124.2	495.4
20ZDC	954.3	113.9	475.5

Table 3
Particle sizes of SP700 Bi_2O_3 powders as a function of ZnO addition.

SP700	Mechanism of particle formation		
	One-particle-per-drop	Nanoparticle agglomeration	
	Mean particle size (nm)	Primary particle size (nm)	Secondary particle size (nm)
Undoped	1016.5	142	727.2
5ZDC	979.1	177.8	550.9
10ZDC	950.4	156.7	542.3
20ZDC	919.5	148.8	545.5

Table 4
Specific surface areas of SP600 and SP700 Bi_2O_3 powders as a function of ZnO addition.

powder	Specific surface area (m^2/g)	
	SP600	SP700
undoped	7.5860	6.7599
5ZDB	5.8950	1.8480
10ZDB	5.9942	4.5211
20ZDB	6.8411	7.4399

Fig. 9. Photocatalytic MO (20 ppm) degradation of SP700 Bi_2O_3 powders under visible light irradiation as a function of ZnO addition. The concentration of catalyst suspended in MO solution is based on the same surface area.

powders, the solid contents of the powders were suspended in organic aqueous solution at a consistent surface area for measurements of the photocatalytic activity. The photocatalytic performance of the SP ZnO-doped Bi_2O_3 powders was evaluated by degrading the MO under visible light irradiation. It should be noted that MO may slightly decompose under visible light irradiation. Meanwhile, physical adsorption also occurs during the process. The MO photodegradation of the powders pyrolyzed at 600 and 700 °C under visible light irradiation, after deducting the degradation effect, is shown in Figs. 8 and 9 as a function of ZnO addition. Furthermore, for comparison, the photocatalytic activity of a
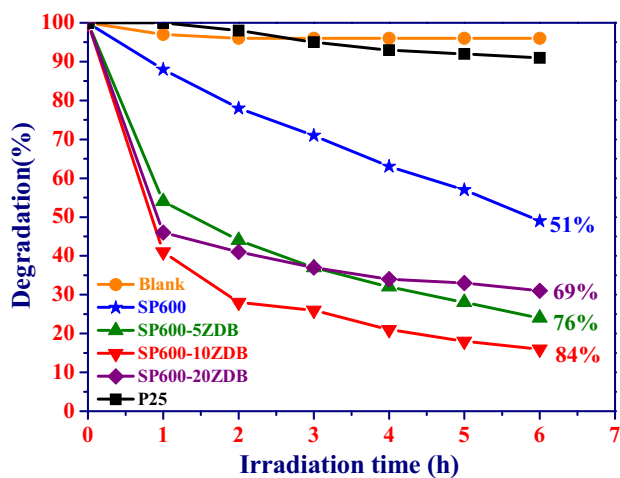
Fig. 8. Photocatalytic MO (methyl orange, 20 ppm) degradation of SP600 Bi_2O_3 powders under visible light irradiation as a function of ZnO addition. The concentration of catalyst suspended in MO solution is based on the same surface area.
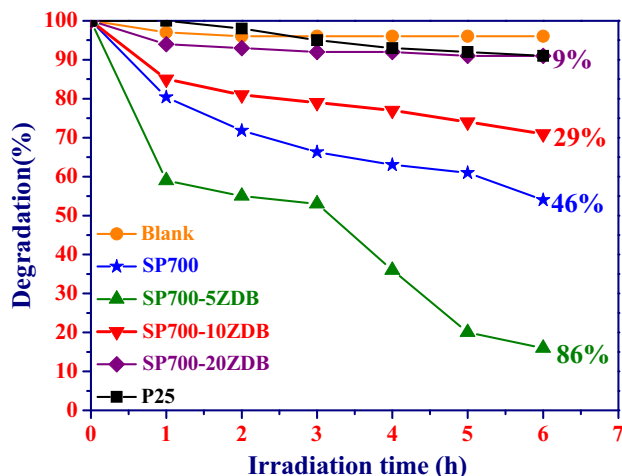
well-known commercial TiO_2 powder (P25, UniRegion Bio-Tech Corp., USA) was evaluated under a visible light source in the same measurement system, although the TiO_2 is an UV-light-activated photocatalyst [14].

As shown in Figs. 8 and 9, the percentage of degradation increased with increases in exposure time. Note that the ZnO-added SP600 powders exhibited obviously greater degradation activity than the unadded equivalent (Fig. 8), showing a better intrinsic photocatalytic activity, though the difference in photocatalytic activity between the ZnO-added samples was not relatively significant. The 10 mol% ZnO-added Bi_2O_3 powder pyrolyzed at 600 °C exhibited the best performance in degrading MO under visible light irradiation for 6 h. This may have resulted from the addition of ZnO, which possesses a larger energy band gap (~3.2 eV) than Bi_2O_3. Recalling the data in Table 1, the band gap of SP Bi_2O_3 powder was increased from ~2.40 eV to ~2.52 eV by adding ZnO. The increase in band gap and lattice defects could effectively cause electron-hole separation inside semiconducting composite materials according to the different band gap structures of their components [15]. The photocatalytic activity of the Zn/Bi oxide powders was thus enhanced. Moreover, the 5 mol% ZnO-added Bi_2O_3 powder pyrolyzed at 700 °C exhibited the best photocatalytic activity in decomposing MO under visible light irradiation. Adding a small amount of ZnO increased the photocatalytic activity of the SP700 Bi_2O_3 powder, and then the activity decreased with further increases in ZnO content. This was believed to result from the more obvious increase in crystallite size of the ZnO-added SP powders pyrolyzed at 700 °C. The commercial TiO_2 powder, P25, exhibited extremely low MO degradation activity under visible light irradiation because the TiO_2 photocatalyst (~3.2 eV energy band gap) should be activated by UV light. In comparison with the commercialized TiO_2 powder, SP ZnO-doped Bi_2O_3 powder, which has a relatively good photocatalytic performance, can degrade MO under visible light irradiation, revealing it to be a potential material for photocatalytic applications.

4. Conclusions

Bi_2O_3 powders with various ZnO additions were prepared by spray pyrolysis at 600 and 700 °C. The XRD data showed that the obtained SP powder transformed from β-type Bi_2O_3 phase into a Zn/Bi oxide phase as the amount of ZnO addition increased. One-particle-per-drop and nanoparticle agglomeration mechanisms were found to result in different microstructures of Bi_2O_3 particles. The XPS data show that ZnO addition decreased the valence state of bismuth ion. A high specific surface area of the SP powders was obtained due to the unique porous

structure. Based on a consistent specific surface area, however, 5 mol% ZnO addition can significantly increase the photocatalytic efficiency of SP700 Bi_2O_3 powder from 46% to 86% under visible light irradiation for 6 h. Under the same irradiation condition, 10 mol% ZnO addition can increase the efficiency of SP600 from 51% to 84%. The photocatalytic activity of the SP powders is significantly higher than that of P25 powder under visible light irradiation.

Acknowledgements

References

[1] M.R. Hoffmann, S.T. Martin, W. Choi, D.W. Bahnemann, Environmental applications of semiconductor photocatalysis, Chem. Rev. 95 (1995) 69–96.

[2] A. López, D. Acosta, A.I. Martínez, J. Santiago, Nanostructured low crystallized titanium dioxide thin films with good photocatalytic activity, Powder Technol. 202 (2010) 111–117.

[3] S. Chin, E. Park, M. Kim, J. Jurng, Photocatalytic degradation of methylene blue with TiO_2 nanoparticles prepared by a thermal decomposition process, Powder Technol. 201 (2010) 171–176.

[4] S.Y. Chai, Y.J. Kim, M.H. Jung, A.K. Chakraborty, D. Jung, W.I. Lee, Heterojunctioned $BiOCl/Bi_2O_3$, a new visible light photocatalyst, J. Catal. 262 (2009) 144.

[5] L. Zhang, W. Wang, J. Yang, Z. Chen, W. Zhang, L. Zhou, S. Liu, Sonochemical synthesis of nanocrystalline Bi_2O_3 as a visible-light-driven photocatalyst, Appl. Catal. A Gen. 308 (2006) 105–110.

[6] J.C. Yu, J.G. Yu, W.K. Ho, L.Z. Zhang, Preparation of highly photocatalytic active nano-sized TiO_2 particles via ultrasonic irradiation, Chem. Commun. (2001) 1942–1943.

[7] K. Nomura, H. Ohta, K. Ueda, T. Kamiya, M. Hirano, H. Hosono, Thin-film transistor fabricated in single-crystalline transparent oxide semiconductor, Science 300 (2003) 1269–1272.

[8] C.-Y. Tsay, K.-S. Fan, S.-H. Chen, C.-H. Tsai, Preparation and characterization of ZnO transparent semiconductor thin films by sol–gel method, J. Alloys Compd. 495 (2010) 126–130.

[9] J. Tauc, R. Grigorovici, A. Vancu, Optical properties and electronic structure of amorphous germanium, Phys. Status Solidi B 15 (1966) 627–637.

[10] A.C.S. Sabioni, A.M.J.M. Daniel, W.B. Ferraz, R.W.D. Pais, A.-M. Huntz, F. Jomard, Oxygen diffusion in Bi_2O_3-doped ZnO, Mater. Res. 11 (2008) 221–225.

[11] T.T. Kodas, M.J. Hampden-Smith, Aerosol Processing of Materials, Wiley-Vch, New York, 1999, p. 421.

[12] G.L. Messing, S.-C. Zhang, G.V. Jayanthi, Ceramic powder synthesis by spray pyrolysis, J. Am. Ceram. Soc. 76 (1993) 2707–2726.

[13] J. Wu, H. Yang, H. Li, Z. Lu, X. Yu, R. Chen, Microwave synthesis of bismuth nano-spheres using bismuth citrate as a precursor, J. Alloys Compd. 498 (2010) L8–L11.

[14] N. Thanabodeekij, E. Gulari, S. Wongkasemjit, $Bi_{12}TiO_{20}$ synthesized directly from bismuth (III) nitrate pentahydrate and titanium glycolate and its activity, Powder Technol. 160 (2005) 203–208.

[15] S. Balachandran, M. Swaminathan, Facile fabrication of heterostructured Bi_2O_3-ZnO photocatalyst and its enhanced photocatalytic activity, J. Phy. Chem. C 116 (2012) 26306–26312.